Beamforming and Imaging with the BYU/NRAO L-Band 19-Element Phased Array Feed

Karl F. Warnick, Brian D. Jeffs,
Jonathan Landon, Jacob Waldron, David Jones
Department of Electrical and Computer Engineering
Brigham Young University, Provo, UT, USA
Email: warnick@ee.byu.edu

J. Richard Fisher and Roger Norrod
National Radio Astronomy Observatory
Charlottesville, VA and Green Bank, WV, USA

***Abstract*—An experimental 19-element L-band phased array feed was installed on the Green Bank 20-Meter Telescope in October 2007 and July 2008 to measure sensitivity and efficiency and demonstrate signal processing algorithms for array calibration, multiple beam formation, imaging, and adaptive spatial filtering methods for interference mitigation. System noise performance was characterized using a warm absorber/cold sky Y-factor setup. The peak beam aperture efficiency was 69% and the minimum beam equivalent system temperature was 66 K. With a single reflector pointing, a high sensitivity image of a field of view approximately two half-power beamwidths in diameter can be produced. Measured figures of merit compare well to numerical simulations, indicating that complicating effects such as mutual coupling are understood well enough to enable the next phase of array feed development to proceed on firm grounds.**

I. Introduction

Phased array feeds (PAFs) promise to increase survey speeds for a variety of astronomical observations, particularly transient source searches and other applications for which rapid sky coverage is advantageous. This will enable more efficient use of limited observation time for large radio telescopes. Research and development issues associated with PAFs include characterization and optimization of sensitivity and system noise temperature, dealing with mutual coupling effects, array calibration, and back-end signal processing.

An experimental 19 element phased array feed was deployed in October 2007 and July 2008 on the NRAO Green Bank 20-Meter Telescope, in order to demonstrate sensitivity-optimized beamforming, "radio camera" imaging with multiple beams, and adaptive spatial filtering algorithms for interference mitigation. Of particular emphasis in these experiments was the development of measurement techniques for aperture efficiency and system noise and careful validation of numerical models for the array and receiver front ends. These results build on earlier work reported by the authors in [1]–[3].

II. PAF Calibration and System Characterization

The phased array feed consisted of 19 thickened dipole elements backed by a ground plane in a hexagonal array with $0.6\,\lambda$ spacing at 1600 MHz (Figure 1). Each element is terminated by an uncooled LNA with nominal minimum noise temperature $T_{\min} = 33\,\mathrm{K}$. A tunable multichannel receiver and data acquisition back-end were used to acquire data and continuously stream raw samples to disk. Beam formation and signal processing were performed in post-processing.

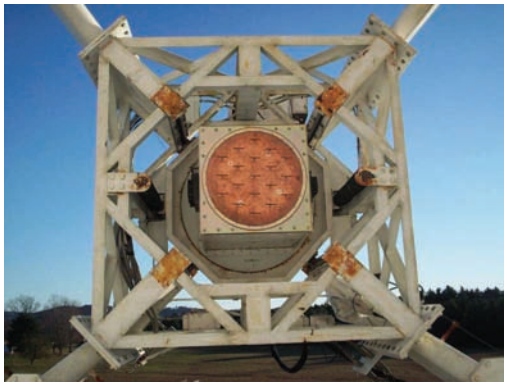

Fig. 1: Phased array feed and front-end box mounted on Green Bank 20-Meter Telescope (October, 2007).

A. Calibration and Beamforming

Beamforming was accomplished using the fixed-adaptive method proposed in [3]. The array was calibrated using a grid of pointings over a field including a bright calibrator source (Cygnus A). The array output correlation matrix $\mathbf{R}_{\mathrm{on},j}$ for each pointing was computed, and one representative correlation matrix $\mathbf{R}_{\mathrm{off}}$ was acquired with the reflector steered several degrees away from the source to estimate the noise field. Integration time was 10 sec. The signal correlation matrix for each pointing was approximated by

$$\mathbf{R}_{\mathrm{s},j} \simeq \mathbf{R}_{\mathrm{on},j} - \mathbf{R}_{\mathrm{off}} \tag{1}$$

A signal steering vector $\mathbf{d}_{\mathrm{s},j}$ for the jth pointing direction was obtained from the dominant eigenvector of $\mathbf{R}_{\mathrm{on},j} - \mathbf{R}_{\mathrm{off}}$. The steering vectors provided a calibration set which was used to form multiple beams over the array field of view. Experimental results show that calibrations are stable for several days or more, even for receiver chains that are not temperature-stabilized.

During an observation, the calibration vectors are used with the maximum-sensitivity beamforming algorithm

$$\mathbf{w}_j = \mathbf{R}_{\mathrm{off}}^{-1}\mathbf{d}_{\mathrm{s},j} \tag{2}$$

978-1-4244-2980-6/09/$25.00 ©2009 IEEE

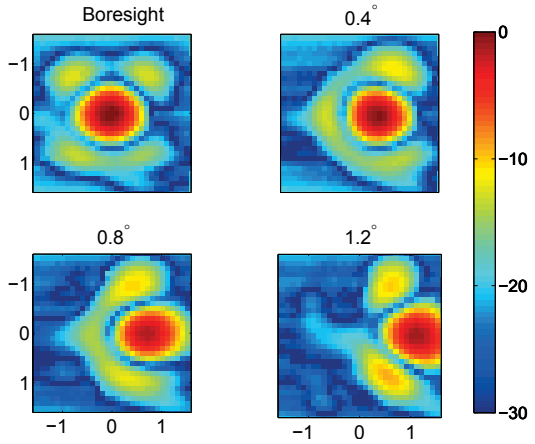

Fig. 2: Measured beam receiving patterns (dB relative to peak).

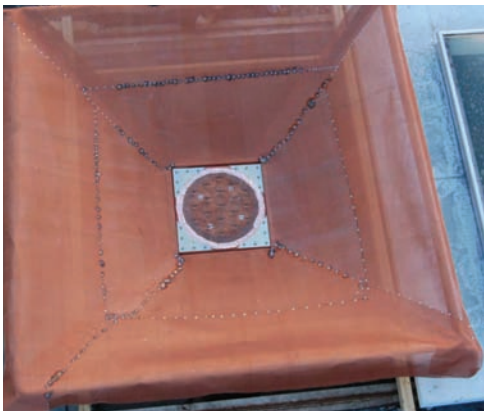

Fig. 3: Ground shield and PAF in sky noise measurement facility (July, 2008).

to compute a set of complex beamformer weights for each calibration grid pointing. $\mathbf{R}_{\rm off}$ in this expression can be an off-source pointing acquired during either the observation or calibration phases. Due to changes in the spillover noise field with reflector pointing direction, sensitivity may be slightly better with an off-source correlation matrix acquired during the observation. For each beam, signal plus noise and noise only powers are computed using

$$P_{\rm sig} + P_{\rm n} = \mathbf{w}_j^H \mathbf{R}_{\rm on} \mathbf{w}_j, \quad P_n = \mathbf{w}_j^H \mathbf{R}_{\rm off} \mathbf{w}_j, \qquad (3)$$

The on/off difference produces the value for the jth image pixel in the PAF field of view.

To probe the receiving pattern of one beam, the reflector can be steered to a grid of pointings similar to that used to calibrate the array. The signal power received by the beam for each pointing provides the beam receiving pattern. Patterns for several steered beams are shown in Figure 2. The sidelobe level is better than 10 dB for steered up to 0.6 degree from boresight. For images requiring tighter sidelobe control, the calibrations could be used to design a beam with controlled pattern shape, but in this paper the maximum-sensitivity beams are used exclusively.

B. Beam Sensitivity, Aperture Efficiency and System Temperature

For a phased array, all figures of merit including sensitivity, efficiencies, and system temperature are beam-dependent. For one beam, the IEEE standard definition of aperture efficiency can be extended to [4]

$$\eta_{\rm ap} = \frac{k_b T_{\rm iso} B}{A_{\rm ap} S^{\rm sig}} \frac{\mathbf{w}^H \mathbf{R}_{\rm sig} \mathbf{w}}{\mathbf{w}^H \mathbf{R}_{\rm iso} \mathbf{w}} \qquad (4)$$

where $\mathbf{R}_{\rm iso}$ is the correlation matrix of the array output voltages due to an isotropic external noise field at temperature $T_{\rm iso}$, B is the system noise equivalent bandwidth, $S^{\rm sig}$ (W/m^2) is the signal of interest flux density in one polarization, $\mathbf{R}_{\rm sig}$ is the array output correlation matrix due to the signal, $A_{\rm ap}$ is the physical aperture area, and $\mathbf{w}$ is a vector of complex beamformer weight coefficients. The beam equivalent system noise temperature is

$$T_{\rm sys} = T_{\rm iso} \frac{\mathbf{w}^H \mathbf{R}_{\rm n} \mathbf{w}}{\mathbf{w}^H \mathbf{R}_{\rm iso} \mathbf{w}} \qquad (5)$$

where $\mathbf{R}_{\rm n}$ is the noise correlation matrix of the receiver noise (estimated by $\mathbf{R}_{\rm off}$).

These definitions have motivated the development of a new measurement technique for array feeds. In order to determine beam efficiencies and system temperature, the response of the array to an isotropic external noise field must be known. This can be measured using an array Y-factor technique. Using a 10 ft^2 copper screen ground shield (Figure 3), the array output correlation matrix $\mathbf{R}_{\rm cold}$ for an isotropic cold source (sky) and $\mathbf{R}_{\rm hot}$ with the array aperture covered by microwave absorber at ambient temperature were acquired. The isotropic noise response of the array is

$$\mathbf{R}_{\rm iso} = \frac{T_{\rm iso}}{T_{\rm hot} + T_{\rm cold}} (\mathbf{R}_{\rm hot} - \mathbf{R}_{\rm cold}) \qquad (6)$$

When the array feed is mounted on the reflector, the difference in integrated beam output powers for on-source and off-source pointings can be used in (4) together with (6) to compute the beam aperture efficiency.

Antenna range measurements could also be used to obtain these parameters, but because the element patterns are far less symmetric than the pattern of a standard feed due to mutual coupling and element displacement, accurate pattern integrations would require pattern samples over a full hemisphere, making the isotropic sky facility more efficient.

By making careful comparisons of measured warm absorber/cold sky responses for single and multiple dipoles to modeled results, the temperatures obtained using this technique appear to be accurate to 5 K. This figure includes sources of systematic measurement error, including sky temperature nonuniformity and ground noise leakage, as well as the effects of errors and simplifications in the numerical model.

Table I shows the sensitivity, aperture efficiency, and system temperature for the center element beam (i.e., $\mathbf{w}^T =$

TABLE I: Measured and modeled peak beam sensitivity, system temperature, and aperture efficiency.

	Center Element	Formed Beam	Model
Sensitivity	$2\,\mathrm{m}^2/\mathrm{K}$	$3.3\,\mathrm{m}^2/\mathrm{K}$	$3.7\,\mathrm{m}^2/\mathrm{K}$
T_{sys}	101 K	66 K	69 K
η_{ap}	64%	69%	81%

TABLE II: System noise budget.

LNA T_{min}	33 K
Mutual coupling	20 K
Spillover	5 K
Sky	3 K
Loss	5 K
Total	66 K

$[1\ 0\ \ldots\ 0]$) and the full-array formed beam with peak sensitivity. The aperture efficiency of the formed beam is 5% larger than that of the center element beam, but the system noise decreases by 35%. The primary contribution to the decreased system noise is the higher spillover efficiency of the maximum sensitivity beam. Modeled results from a finite element method (FEM) numerical model of the array using HFSS (Ansoft Corp.) coupled with network theory for the LNAs and receiver chains are also shown in the table. Element losses are included in the model as a 5 K contribution to the beam equivalent system temperature.

The system noise budget for a formed beam is shown in Table II. The total beam equivalent system noise temperature was computed with (5) from an on-reflector noise response measurement and the array isotropic noise response obtained with the warm absorber/cold sky setup. The noise contribution from ohmic losses in the elements was estimated from the measured loss of the coaxial dipole element support structure. The remaining contributions were estimated using the numerical model. The mutual coupling contribution is caused by mismatch between the LNA optimal source impedance and the beamformer-dependent active impedances presented by the PAF to the amplifiers [5].

Beam sensitivity can be mapped with a grid of calibrator source pointings. For each beam, an off-source pointing and an on-source pointing with the reflector steered so that the beam is centered on the source were used to compute SNR, which can be converted to sensitivity using the known source flux density. A map of beam sensitivities is shown in Figure 4. The 1 dB field of view is roughly 2 HPBW in diameter.

Figure 5 shows a slice through the sensitivity map with a comparison to the model results. The measured PAF beam sensitivity is approximately 90% of the modeled value. The measured aperture efficiency is lower than the modeled value by 12%, due in part to reflector blockage and feed support scattering, which are not taken into account in the model.

III. Imaging

Figure 6 shows a mosaic of images of the Cygnus X region at 1600 MHz. The mosaic was assembled from 25 1.6 × 1.6 degree image tiles on a 5 × 5 grid. Each tile represents a single reflector pointing. A 17 × 17 pixel image is obtained for each pointing by forming multiple beams electronically. For a single-pixel feed with a raster spacing of one half the half-power beamwidth, approximately 600 pointings would be required to form a similar image, so the imaging speedup with the PAF assuming identical sensitivities is a factor of 24.

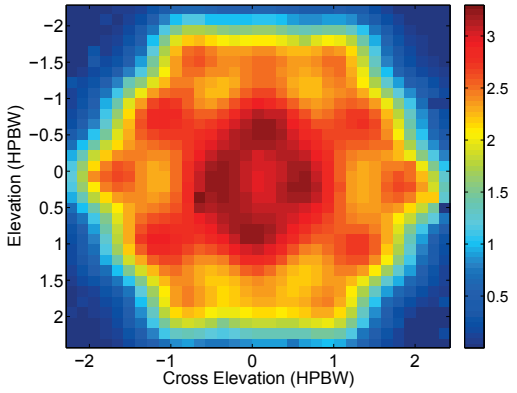

Fig. 4: Beam sensitivity map (m^2/K). Each pixel in the image corresponds to the measured sensitivity of one formed beam. The half-power beamwidth (HPBW) of the 20-Meter telescope is 0.7 degrees.

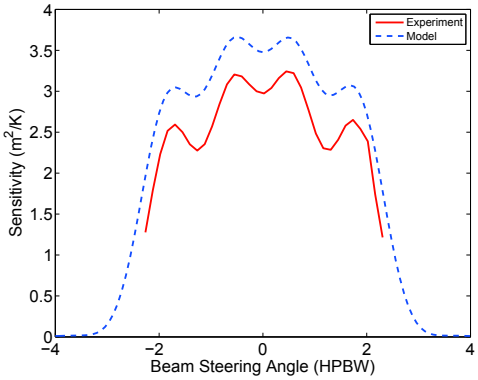

Fig. 5: Measured and modeled beam sensitivity for an elevation cut.

A. RFI Mitigation

Array feeds enable the use of spatial filtering algorithms for adaptive RFI mitigation [1]. This capability comes at the cost of increased signal processing complexity and data rates, since integration dump times on the order of tens of milliseconds are required to track rapidly moving RFI sources. To demonstrate the feasibility of adaptive RFI mitigation, an FM-modulated RFI source overlapping the W3OH spectral line at 1665 MHz was created artificially using a signal generator and small horn antenna. The RFI was removed using the subspace projection algorithm [7]. Images of the source with and without RFI mitigation are shown in Figure 7. Some distortion due to residual RFI is apparent in Figure 7(c) after

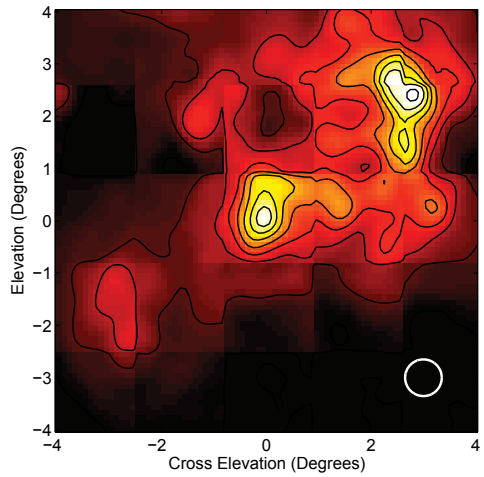

(a) 5 × 5 mosaic of PAF images. The circle indicates the half-power beamwidth.

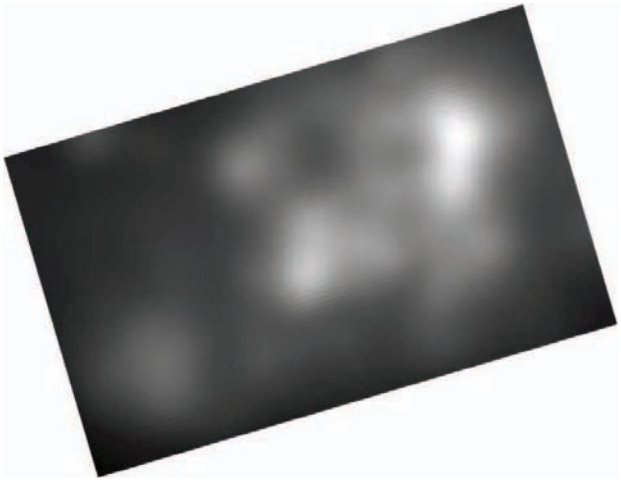

(b) Canadian Galactic Plane Survey image [6] convolved to 20-Meter beam.

Fig. 6: Cygnus X region at 1600 MHz.

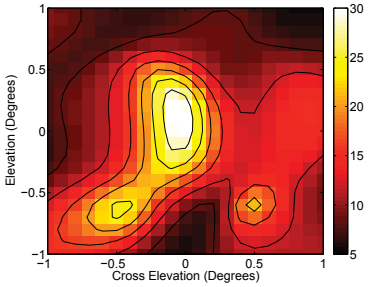

(a) No RFI.

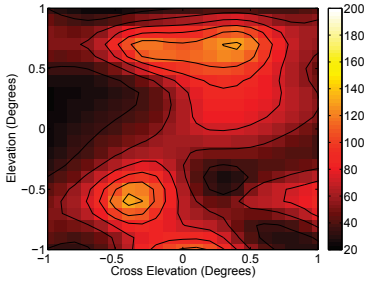

(b) With RFI.

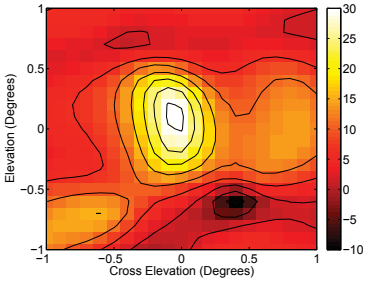

(c) With RFI, adaptive spatial filtering using subspace projection.

Fig. 7: W3OH image with and without RFI. The color scale is equivalent antenna temperature (K).

adaptive processing, but the source is clearly visible in the image.

IV. Conclusion

The experimental results and images presented in this paper represent some of the first ever reported for an on-reflector phased array feed, and demonstrate that significant progress has been made towards the realization of a PAF with astronomically useful sensitivity. A practical approach to array calibration and beamforming has been demonstrated, and a measurement technique approach which allows the aperture efficiency and system temperature of the phased array feed to be characterized has been developed. Measured beam sensitivity, efficiency, and system noise temperature agree with simulated results to within expected tolerance, indicating that complicating effects such as mutual coupling are understood well enough to enable the next phase of PAF development to proceed on firm grounds. Challenges for future work include active impedance matching to reduce the noise penalty associated with mutual coupling and the development of cryogenic elements and front-ends.

References

[1] J. R. Nagel, K. F. Warnick, B. D. Jeffs, J. R. Fisher, and R. Bradley, "Experimental verification of RFI mitigation with a focal plane array feed," *Radio Science*, vol. 42, doi:10.1029/2007RS003630, 2007.

[2] K. F. Warnick, B. D. Jeffs, J. Landon, J. Waldron, D. Jones, and A. Stemmons, "BYU/NRAO 2007 Green Bank 20 Meter Telescope focal plane array - modeling and experimental results," invited presentation, SKADS MCCT Technical Workshop on Design of Wideband Receiving Array Systems, Dwingeloo, The Netherlands, Nov. 26-30, 2007.

[3] B. D. Jeffs, K. F. Warnick, J. Landon, J. Waldron, D. Jones, J. R. Fisher, and R. Norrod, "Signal processing for phased array feeds in radio astronomical telescopes," *IEEE Journal of Selected Topics in Signal Processing*, in press, 2008.

[4] K. F. Warnick and B. D. Jeffs, "Beam efficiencies and system temperature for a focal plane array," *IEEE Antennas and Wireless Propagation Letters*, in press, 2008.

[5] E.E.M. Woestenburg, "Noise matching in dense phased arrays," ASTRON, Dwingeloo, The Netherlands, Tech. Rep. RP-083, Aug. 2005.

[6] A. R. Taylor et al., "The Canadian Galactic Plane Survey," *Astronomical Journal*, vol. 125, pp. 3145–3164, June 2003, http://www.ras.ucalgary.ca/CGPS/products/.

[7] A. Leshem, A.-J. van der Veen, and A.-J. Boonstra, "Multichannel interference mitigation techniques in radio astronomy," *Astrophysical Journal Supplements*, vol. 131, no. 1, pp. 355–374, 2000.